# ILETA International Information and Engineering Technology Association

# International Journal of Design & Nature and Ecodynamics

Vol. 20, No. 9, September, 2025, pp. 2049-2058

Journal homepage: http://iieta.org/journals/ijdne

# Modified Meerschaum for Removal of Methylene Blue Dye from Aqueous Solutions: Characterization, Adsorption Behavior, Performance Evaluation



Morad Abdulwheed Radha<sup>1\*</sup>, Zainab Mohammed Ameen Ahmed<sup>2</sup>, Havva Tutar Kahraman<sup>3</sup>, Erol Pehlivan<sup>3</sup>, Mohammed Qader Gubari<sup>1</sup>

- <sup>1</sup> Fuel and Energy Techniques Engineering Department, College of Oil and Gas Techniques Engineering/Kirkuk, Northern Technical University, Kirkuk 36001, Iraq
- <sup>2</sup> Department of Basic Sciences, College of Nursing, University of Kirkuk, Kirkuk 36001, Iraq

Corresponding Author Email: morad.a.radha@ntu.edu.iq

Copyright: ©2025 The authors. This article is published by IIETA and is licensed under the CC BY 4.0 license (http://creativecommons.org/licenses/by/4.0/).

https://doi.org/10.18280/ijdne.200910

Received: 16 July 2025 Revised: 20 August 2025 Accepted: 25 August 2025

Available online: 30 September 2025

#### Keywords:

modified nano-adsorbent, meerschaum, methylene blue removal, characterization, equilibrium, kinetics

# **ABSTRACT**

This study investigates the removal of methylene blue (MB), a cationic dye, from aqueous solutions using modified nano-meerschaum (mod-nM/3APTS) functionalized with 3-aminopropyl triethoxysilane. Structural characterization by FTIR, EDX, and TEM confirmed the successful modification and improved surface activity. Batch adsorption experiments revealed that equilibrium was reached within 120 minutes, with adsorption efficiency strongly influenced by pH, adsorbent dosage, and initial MB concentration. The maximum adsorption capacity was 127.75 mg/g, consistent with the Langmuir isotherm model, indicating monolayer chemisorption. Kinetic studies showed that the adsorption process followed the pseudo-second-order model, while thermodynamic analysis confirmed that MB adsorption was spontaneous and endothermic. Furthermore, mod-nM/3APTS exhibited good regeneration performance, maintaining over 88% efficiency after five reuse cycles. These findings demonstrate that mod-nM/3APTS is a low-cost, reusable, and highly effective adsorbent for dye removal in wastewater treatment applications.

# 1. INTRODUCTION

The discharge of synthetic dyes into water bodies through industrial effluents poses a serious environmental and public health threat. Dyes are extensively used in the textile, paper, printing, pharmaceutical, and plastic industries, and their direct release into aquatic environments leads to high organic loading and persistent contamination. Many of these compounds, including methylene blue (MB), are toxic and carcinogenic, causing harmful effects such as increased heart rate, diarrhea, quadriplegia, and long-term ecological damage. Consequently, dye pollution remains a critical environmental challenge requiring efficient and sustainable treatment solutions [1].

Various methods have been employed for dye removal from wastewater, including ion exchange, reverse osmosis, biological remediation, membrane separation, catalytic degradation, and adsorption [2-8]. Kıpçak et al. [9] demonstrated the potential of Turkish sepiolite samples, nodular sepiolite (NS) and industrial sepiolite (IS) for the removal of Ni<sup>2+</sup> ions. Their study revealed that sepiolite's high surface area and porosity enabled effective adsorption under optimized conditions (pH 6, 0.6 g/50 mL dosage). Adsorption followed the Freundlich isotherm and pseudo-second-order kinetics, confirming a chemisorption process. Furthermore, the process was spontaneous and endothermic, with the

materials showing strong reusability through multiple adsorption-desorption cycles. This work confirmed sepiolite's suitability as a low-cost adsorbent for heavy metal removal.

Expanding on combined pollutant scenarios, Rosales et al. [10] explored a hybrid system integrating NaY zeolite and the bacterium Arthrobacter viscosus for simultaneous dye (Azure B) and metal (Cr(VI)) removal. The results indicated synergistic effects, achieving >99% dye removal and >50% Cr(VI) removal within 8 days. Adsorption kinetics followed a pseudo-second-order model, while equilibrium data fitted best with the Redlich-Peterson isotherm. This study highlighted the importance of hybrid systems that combine inorganic and biological mechanisms to address complex wastewater contamination.

Complementary advances in biopolymer–clay composites have further enhanced dye adsorption efficiency. Wang et al. [11] developed cellulose/montmorillonite (MTM) hydrogels, achieving a maximum methylene blue (MB) adsorption capacity of 277 mg/g, significantly higher than MTM alone. Adsorption was dominated by physisorption within the hydrogel's internal structure, suggesting that the clay–biopolymer matrix enhances accessibility of adsorption sites. Owing to its biodegradability, high efficiency, and scalability, the cellulose/MTM hydrogel presents strong potential for sustainable dye wastewater treatment.

Taking the innovation further, Kumari et al. [12]

<sup>&</sup>lt;sup>3</sup> Department of Chemical Engineering, Konya Technical University, Konya 42079, Turkey

synthesized bio-based polyurethane foams (PUFs) from cellulose nanowhiskers derived from pine needles. These foams exhibited exceptional adsorption capacity for MB (554.8 mg/g), with near-complete dye removal achieved within 20 minutes at 55°C. Importantly, the PUFs demonstrated excellent reusability over multiple cycles, combining rapid kinetics with cost-effectiveness and environmental sustainability. While effective under certain conditions, these methods often face limitations such as high operational costs, secondary waste generation, or reduced efficiency in treating dilute or complex dye mixtures. Among these approaches, adsorption has emerged as one of the most promising techniques due to its simplicity, cost-effectiveness, and adaptability for large-scale treatment.

Natural adsorbents, particularly clays and related minerals, have attracted considerable attention as eco-friendly and inexpensive alternatives. Materials such as montmorillonite, polyurethane foam, biochar, palygorskite, clinoptilolite, and sepiolite (meerschaum) have been successfully explored for dye removal. Yu et al. [13] developed a novel porous adsorbent using modified sepiolite-stabilized Pickering foams as templates, avoiding the excessive use of organic solvents typical of high internal phase emulsions (HIPEs). The resulting material exhibited excellent pore stability across a wide pH range (4-11) and outstanding adsorption performance, with maximum capacities of 1421.18 mg/g for methylene blue and 638.81 mg/g for methyl green at 25°C. These findings highlight the potential of sepiolite-based porous structures for rapid and selective dye removal, providing an eco-friendly approach for wastewater treatment. Gong et al. [14] investigated the pyrolysis of ramie residues collected after phytoremediation of heavy contaminated1sediments. Pyrolysis at 300-700°C stabilized 1Cd, Cr, Zn, Cu, and Pb by transforming their acid-soluble fractions into more stable residual forms, thereby reducing leachability. Importantly, the pyrolysis products also exhibited high potential as adsorbents, achieving a maximum methylene blue (MB) adsorption capacity of 1259.27 mg/g. This dual benefit stabilization of toxic metals and reutilization of residues as dye sorbents demonstrates pyrolysis as a circular approach to waste valorization.

Similarly, He et al. [15] focused on palygorskite clays purified through suspension precipitation using sodium hexametaphosphate. The purification effectively removed associated minerals such as quartz and dolomite, enhancing the adsorption properties of palygorskite. The purified material exhibited an MB adsorption capacity of 219.69 mg/g, with adsorption kinetics following a pseudo-second-order model. Mechanistic analysis suggested that MB removal was governed by electrostatic attraction to negatively charged surfaces, supplemented by hydrogen bonding between palygorskite hydroxyl groups and MB's heteroatoms. These findings underscore the effectiveness of mineral purification in improving dye adsorption performance.

In contrast, Çoruh et al. [16] explored the adsorption capabilities of two natural minerals, sepiolite and clinoptilolite, for crystal violet and Congo red removal. Using a central composite experimental design, the study demonstrated that sepiolite achieved up to 99% removal efficiency for both dyes, outperforming clinoptilolite, which showed limited effectiveness for Congo red. This highlights the selective adsorption behavior of different natural clays and emphasizes the importance of matching adsorbents to specific pollutants.

In contrast, Zhuang et al. [17] investigated the role of organic surfactants in tailoring the structure and rheological properties of organo-sepiolite (OSep) for oil-based drilling fluids. Their results showed that surfactants partially insert into sepiolite channels, blocking micropores and reducing specific surface area while enhancing fiber dispersion, rheological behavior, and thermal stability. This study emphasized the significance of surfactant size in determining structural interactions and demonstrated sepiolite's adaptability as a rheological modifier in energy-related industries.

Complementing these functional studies, Raya et al. [18] provided fundamental structural insights into sepioliteorganic complexes by applying advanced two-dimensional 1H-29Si HETCOR spectroscopy. Their work confirmed that indigo molecules penetrate the sepiolite structure, interacting with water coordinated to magnesium ions rather than surface silanol groups. This provided the first direct spectroscopic evidence for the structural basis of the historical Maya Blue pigment and clarified the nature of sepiolite-indigo interactions. Their fibrous morphology, porous structure, and surface functional groups enable strong interactions with organic contaminants. Sepiolite, a hydrated magnesium silicate with interconnected channels and abundant silanol groups, is especially notable for its lightweight structure, high surface reactivity, and multiple active adsorption zones [19]. However, pristine sepiolite suffers from limited surface area and insufficient reactive groups, which restrict its dye adsorption efficiency.

To overcome these drawbacks, surface modification strategies have been developed to enhance adsorption capacity. Functionalization with 3-aminopropyl triethoxysilane (3APTS) introduces amine groups that improve the interaction between sepiolite and cationic dyes, thereby significantly enhancing adsorption performance.

The present study aims to evaluate the adsorption behavior of modified nano-meerschaum (mod-nM/3APTS) for the removal of methylene blue from aqueous solutions. The work systematically investigates the influence of pH, contact time, adsorbent dosage, and dye concentration, supported by kinetic, isotherm, and thermodynamic analyses. The findings provide new insights into the potential of functionalized sepiolite as a low-cost, efficient, and reusable adsorbent for 1 wastewater treatment.

#### 2. MATERIALS AND METHODS

Meerschaum, sodium hydroxide (NaOH), and hydrochloric acid (HCl) were obtained from Sigma-Aldrich. Acidic and basic solutions were employed to adjust the pH of all prepared solutions. A single needle-like meerschaum fiber typically exhibits dimensions ranging from 0.2 to 4  $\mu m$  in length, 10 to 30 nm in width, and 5 to 10 nm in thickness. The material also contains open nanochannel voids with dimensions of 3.5 Å  $\times$  10.6 Å [20]. All reagents used in the adsorption experiments were of analytical grade, and ultrapure water produced by a Millipore Direct-Q® 3 UV Water Purification System was used throughout. A standard dye solution was prepared by dissolving 1.0 g of methylene blue (MB) in 1 L of ultrapure water. Samples for adsorption experiments were subsequently agitated in an incubated shaker to ensure homogeneous mixing.

# 2.1 Natural meerschaum modification procedure

To prepare the modified adsorbent, 10 g of natural nanomeerschaum (nM) was combined with 3 mL of 3-(aminopropyl) triethoxysilane and 100 mL of a methanol/water solution (90:10) in a 250 mL two-necked flask equipped with a condenser. The mixture was refluxed under a nitrogen atmosphere with continuous stirring for 20 hours. After completion, the solid phase was recovered by centrifugation at 1000 rpm and rinsed three times with acetone. The resulting modified meerschaum (mod-nM/3APTS) was dried at 90°C for 1 hour before further use.

# 2.2 FTIR interpretation of the modified meerschaum (mod-nM/3APTS) and modified meerschaum adsorbed methylene blue (mod-nM/3APTS /MB)

The FTIR spectra of nM, mod-nM/3APTS, and (modnM/3APTS)/MB are presented in Figure 1(a-d). In the spectrum of nM (Figure 1(a)), characteristic absorption bands at 3610 and 3564 cm<sup>-1</sup> correspond to the stretching vibrations of Mg-OH groups, while the band at 3417 cm<sup>-1</sup> is attributed to hydrogen-bonded hydroxy groups and adsorbed water. The peak at 1660 cm<sup>-1</sup> represents bending vibrations of molecular water coordinated with magnesium, and the strong bands observed at 1018 and 1203 cm<sup>-1</sup> are assigned to Si-O and Si-O-Si stretching vibrations of the silicate framework. The band at 648 cm<sup>-1</sup> corresponds to Mg-OH bending vibrations. After modification with 3APTS (Figure 1(b)), new features emerge, including the appearance of a C-H stretching band at 2931 cm<sup>-1</sup>, confirming the incorporation of organic groups from the modifier. The slight shifts in the hydroxyl bands (3556 and 3425 cm<sup>-1</sup>) and changes in the intensity of Si-O bands further indicate successful surface functionalization. Following MB adsorption onto the modified adsorbent (Figure 1(c)), new peaks appear at 1011 and 974 cm<sup>-1</sup>, while the broad -OH region shows a notable reduction in intensity, suggesting strong interactions between MB and the surface functional groups. The peaks near 1606 and 1203 cm<sup>-1</sup> become sharper, reflecting the contribution of MB aromatic and C-N groups. These spectral changes collectively confirm that MB molecules were effectively adsorbed onto the mod-nM/3APTS surface through electrostatic interactions, hydrogen bonding, and possible chemisorption mechanisms. In Figure 1(d), the pristine nM spectrum shows characteristic bands of hydroxyl and silicate groups, including broad peaks in the region of 3600-3400 cm<sup>-1</sup> attributed to -OH stretching vibrations, a band at ~1660 cm<sup>-1</sup> associated with adsorbed water, and strong Si-O and Si-O-Si stretching vibrations around 1200-1000 cm<sup>-1</sup>. After surface modification with 3APTS, the mod-nM/3APTS spectrum exhibits a new band at ~2930 cm<sup>-1</sup> corresponding to C-H stretching l vibrations, confirming the successful grafting of organic groups. Slight shifts in the hydroxyl bands and variations in Si-O peak intensities further support the functionalization of meerschaum. In contrast, the spectrum of MB-loaded mod-nM/3APTS shows significantly reduced intensity of the hydroxyl stretching region, along with distinct peaks near 1600–1200 cm<sup>-1</sup> that overlap with MB aromatic and C-N vibrations. These changes indicate strong electrostatic and hydrogen bonding interactions between MB and the amine-functionalized surface. This observation supports and aligns with results reported in prior studies [21-25].

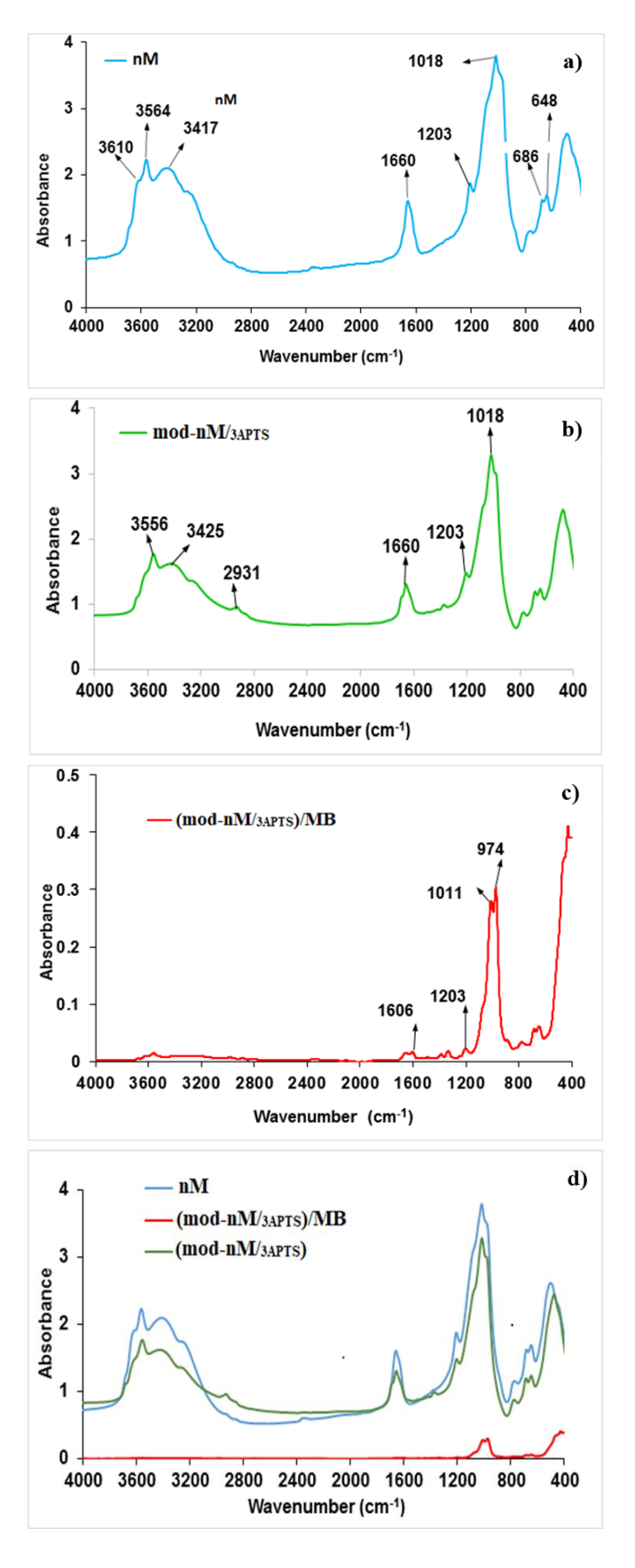


**Figure 1.** FTIR spectra of (a) pristine nano-meerschaum (nM), (b) modified nano-meerschaum with 3-aminopropyl triethoxysilane (mod-nM/3APTS), (c) methylene blue-loaded modified nano-meerschaum ((mod-nM/3APTS)/MB), and (d) comparative overlay of nM, mod-nM/3APTS, and (mod-nM/3APTS)/MB

# 2.3 Energy dispersive X-ray spectrometer (EDX)

The chemical composition1percentages of the utilized meerschaum were characterized by EDX analysis. Figure 2 presents the SEM micrograph and EDX spectrum of nM. The SEM image reveals the characteristic fibrous and porous morphology of meerschaum, with needle-like structures forming a loosely packed network. This fibrous arrangement provides a high surface area and abundant channels, favorable for adsorption processes. The morphology confirms the nanoscale features of the material, with fibers and plate-like fragments distributed across the surface.

The corresponding EDX spectrum confirms the elemental composition of nM, showing prominent peaks for magnesium (Mg), silicon (Si), and oxygen (O), which are the primary constituents of meerschaum, consistent with its chemical formula (Si<sub>12</sub>Mg<sub>8</sub>O<sub>30</sub>(OH)<sub>4</sub>(OH<sub>2</sub>)<sub>4</sub>·8H<sub>2</sub>O). Minor traces of other elements may also be detected, likely originating from impurities or natural mineral inclusions. The strong presence of Si and Mg peaks validates the silicate framework, while the O peak reflects both structural oxygen and surface hydroxyl groups.

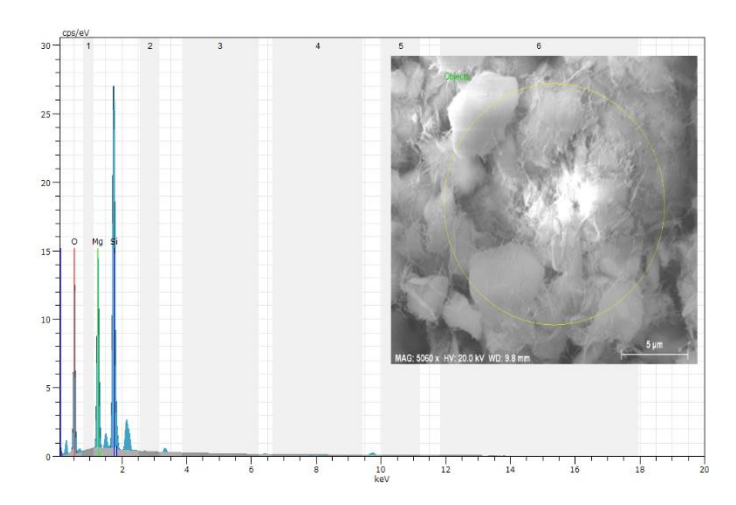


Figure 2. SEM/EDX analysis of nM

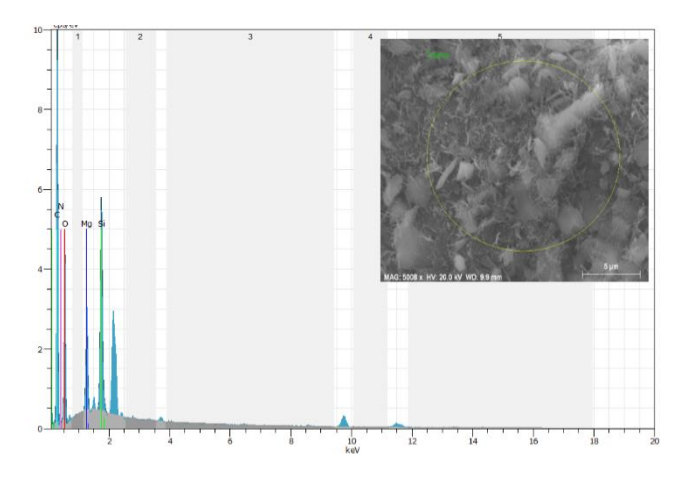


Figure 3. SEM/EDX analysis of mod-nM/3APTS

Figure 3 presents the SEM/EDX analysis of mod-nM/3APTS. The SEM micrograph shows a rough and irregular surface morphology, suggesting successful surface modification. The EDX spectrum confirms the presence of key elements, including carbon (C), oxygen (O), and silicon (Si), indicating the successful grafting of 3APTS onto the modified

nanomaterial. The presence of Si is particularly significant as it verifies the silane functionalization, while the absence of major contaminant peaks suggests good sample purity. Together, these results confirm the effective surface functionalization of mod-nM with 3APTS.

Table 1 compares the elemental composition of nM and mod-nM/3APTS. The increase in oxygen content and the appearance of carbon and nitrogen confirm the successful grafting of 3APTS, while the decrease in magnesium and silicon indicates surface coverage by the silane layer.

**Table 1.** Percentage composition of nM and modnM/3APTS

Element (wt%)	nM	Mod-nM/3APTS
Oxygen	67.28	71.6
Magnesium	12.23	5.44
Silicon	20.49	9.47
Nitrogen	-	2.87
Carbon	-	10.61

# 2.4 Transmission electron microscopy (TEM)

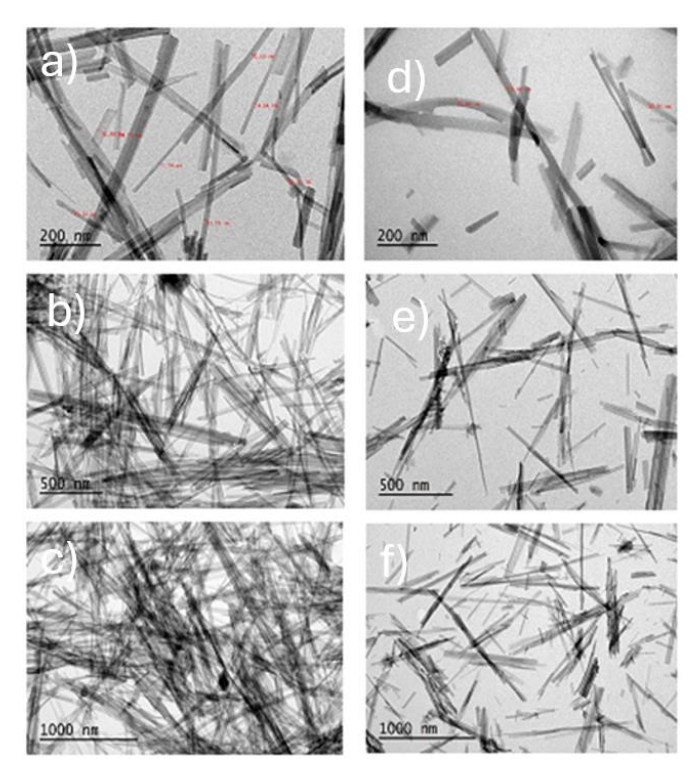


Figure 4. TEM images of nM and mod-nM/3APTS

Figure 4(a-c) shows the TEM images of nM, and Figure 4(d-f) shows the modified meerschaum with 3-aminopropyltriethoxysilane (mod-nM/3APTS). The TEM images of nM reveal a dense and intertwined fibrous structure, where the long fibers are closely packed and form combined networks, exhibiting a typical needle-like nanoscale morphology. In contrast, the mod-nM/3APTS samples display shorter fibers that are less entangled and more separated from each other, indicating that the modification process significantly alters the aggregation behavior of the fibers while maintaining their needle-like nanosized features. To further characterize the samples, a UV-Visible spectrophotometer (Shimadzu UV-1700) was employed to determine the residual dye concentration in adsorption experiments, a pH meter (Orion 900S2) was used for pH measurements, and a GFL

3033 shaker was applied to ensure proper mixing of the adsorbent-dye solutions. Additionally, the functional groups on the adsorbent surfaces were examined using a Bruker VERTEX 70 FTIR spectrometer, and all surface peaks were identified and explained.

# 2.5 Batch equilibrium studies

In the adsorption studies, the modified adsorbent was introduced into batch-vessel reactors containing 100 mL of 0.001 M MB solution, and the mixtures were agitated at 200 rpm under the desired pH and contact times. The residual concentration of MB in the solution after adsorption was determined using a UV-Visible spectrophotometer at a wavelength of 665 nm. The adsorption capacity of the adsorbent, qe (mg/g), was then calculated using the following equations:

Adsorption% = 
$$\frac{\text{Ci} - \text{Cf}}{\text{Ci}} \times 100$$
 (1)

While qe was calculated by Eq. (2):

$$qe = \frac{Ci - Cf}{m} \times V \tag{2}$$

Here, Ci and Cf represent the initial and time-dependent dye concentrations (mg/L), respectively, V is the solution volume (L), and m is the mass of adsorbent (g). The Freundlich isotherm (Eq. (3)), expressed as [26]:

$$\log (qe) = \log K_F + \frac{1}{n} \log Ce$$
 (3)

Eq. (3) is used to describe multilayer adsorption on a heterogeneous surface, where  $K_F$  is the adsorption capacity constant and n indicates adsorption intensity, and Ce is the equilibrium dye concentration (mg/L). In contrast, the Langmuir isotherm (Eq. (4)):

$$\frac{\text{Ce}}{\text{ge}} = \frac{1}{O_0 K_L} + \frac{1}{O_0} \text{Ce} \tag{4}$$

Assumes monolayer adsorption on a homogeneous surface, with  $Q_0$  representing the maximum adsorption capacity (mg/g) and  $K_L$  the Langmuir constant related to adsorption affinity (L/mg). Together, these models provided insight into the adsorption mechanisms governing the interaction between the adsorbent and dye molecules [27, 28].

In this study, the first- and second-order pseudo-kinetic models were utilized to analyze the adsorption process. The pseudo 1 kinetic model, shown in Eq. (5):

$$\log(\text{qe} - \text{qr})1 = 1\log(\text{qe}) - \frac{k_1}{2.303}1t$$
 (5)

The adsorption rate is proportional to the number of unoccupied sites, where qe and qr represent the amounts of adsorbate adsorbed at equilibrium and at time t, respectively, and  $k_1$  (min<sup>-1</sup>) is the pseudo-first-order rate constant. The pseudo-second-order kinetic model, expressed in Eq. (6):

$$\frac{t}{q_t} = \frac{1}{K_2 q_e^2} + \frac{t}{q_e} \tag{6}$$

This equation is based on the assumption that chemisorption is the rate-limiting step, involving valence forces through electron sharing or exchange between the adsorbent and adsorbate. In the pseudo-second-order kinetic model,  $k_2$  (g/mg·min) represents the equilibrium rate constant. The kinetic parameters of this model can be obtained by plotting t/qt against time t. Furthermore, thermodynamic parameters such as Gibbs free energy change ( $\Delta G \circ$ ), enthalpy change ( $\Delta H \circ$ ), and entropy change ( $\Delta S \circ$ ) of adsorption were evaluated using Eqs. (7) and (8). The adsorption equilibrium constant ( $K_{ads}$ ) was employed in the following relation to calculate  $\Delta G \circ$  for the adsorption process at different temperatures.

$$\Delta G^{o} = -RT \ln K_{ads} \tag{7}$$

$$lnK_{ads} = \frac{\Delta H^{o}}{RT} + \frac{\Delta S^{o}}{R}$$
 (8)

The adsorption equilibrium constant ( $K_{ads}$ ) can also be expressed as a function of temperature in terms of  $\Delta H \circ$  in kJ/mol and  $\Delta S \circ$  in J/mol.K. These thermodynamic parameters can be determined from the van't Hoff equation by plotting in  $K_{ads}$  against 1/T, where the slope corresponds to - $\Delta H \circ /R$  and the intercept to  $\Delta S \circ /R$ .

#### 3. RESULTS AND DISCUSSION

#### 3.1 Influence of pH

To investigate the influence of pH on MB adsorption, the pH of the dye solution was adjusted from 2 to 9 using acid and base solutions. The initial pH is a critical factor in adsorption studies, as it governs the solubility of dye molecules, the surface charge of the adsorbent, and the electrostatic interactions between them [29]. In this study, 100 mg/L MB was used as the model solution. The adsorption process is largely controlled by two mechanisms: (i) electrostatic interactions between the functional groups on the adsorbent surface and the dye molecules (outer-sphere complexes) and (ii) ion exchange processes (inner-sphere complexes). These interactions collectively determine the removal efficiency of dyes from aqueous media.

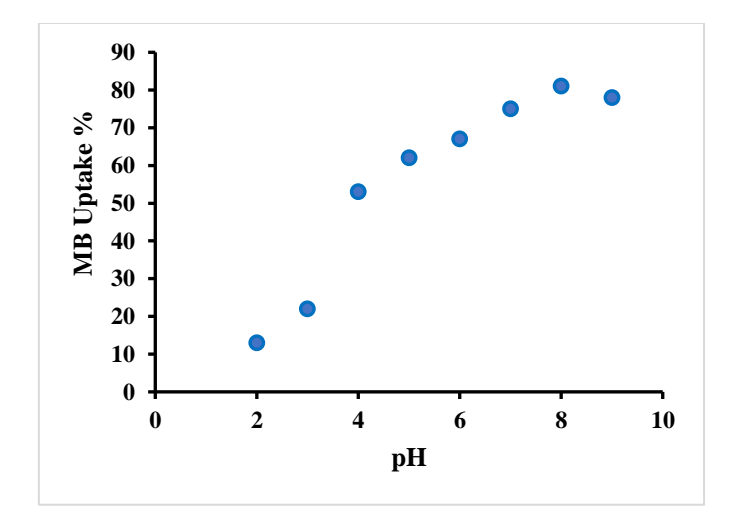


**Figure 5.** Effect of pH on MB removal by modnM/3APTS

As shown in Figure 5, MB adsorption was low at acidic conditions (pH  $\approx$  2). With increasing pH, the adsorption capacity improved significantly, particularly between pH 4 and 7, and reached its maximum near pH 8. Beyond pH 7, no substantial increase in adsorption was observed. This behavior can be explained by the protonation state of the amine (–NH<sub>2</sub>) groups on the modified adsorbent surface. At low pH, these groups are protonated to –NH<sub>3</sub>+, which causes electrostatic repulsion with the cationic dye molecules, thereby reducing adsorption. At higher pH values, deprotonation occurs, reducing surface charge repulsion and favoring dye uptake.

The observed adsorption behavior suggests that both chemisorption and physisorption mechanisms are involved [30, 31]. Chemisorption likely arises from strong, irreversible interactions such as electron sharing or covalent bonding, while physisorption involves weaker interactions,1including hydrogen bonding, dipole—dipole forces, and  $\pi$ – $\pi$  interactions between the dye molecules and the adsorbent surface.

#### 3.2 Effect of contact time

The variation of MB uptake with contact time at pH 7 and constant temperature is shown in Figure 6. The adsorption process displays a rapid initial increase in MB uptake, reaching approximately 55-60% removal within the first hour. This indicates that a large number of active sites on the modnM/3APTS surface are readily available for dye molecules at the start of the process. As the contact time increases to 2 hours, MB uptake reaches about 75-78%, after which the rate of adsorption slows considerably. Beyond 3-4 hours, the adsorption curve begins to plateau at around 80% uptake, signifying that equilibrium has been reached and most of the available adsorption sites have been occupied. Based on these observations, a contact time of 2 hours was selected as the optimal duration for subsequent experiments, since it provides near-equilibrium adsorption with minimal additional uptake beyond this point. The initial rapid adsorption phase can be attributed to the abundance of active sites, while the slower phase reflects the gradual saturation of the adsorbent surface.

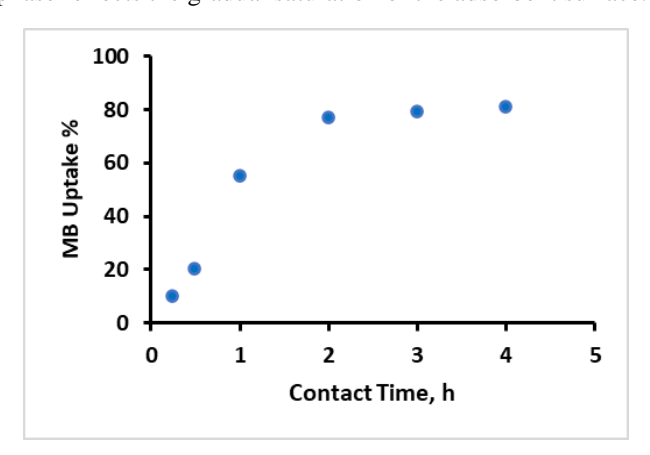


**Figure 6.** Effect of contact time on MB removal by modnM/3APTS

# 3.3 Influence of adsorbent dosage

The effect of adsorbent dosage on MB removal was investigated by varying the amount of mod-nM/3APTS from 0.25 to 2.0 g/L under constant experimental conditions (MB concentration = 1001mg/L, temperature = 251°C, pH = 7). As shown in Figure 7, MB uptake increased sharply with increasing adsorbent dose, rising from approximately 40%

removal at 0.25 g/L to nearly 80% at 0.5 g/L. The maximum adsorption efficiency of about 95–100% MB uptake was achieved at a dose of 1.0 g/L, beyond which further increases in adsorbent dose produced no significant improvement. This plateau behavior indicates that almost all available MB molecules were adsorbed at 1.0 g/L, suggesting that the active sites were sufficiently abundant at this dosage. Therefore, 1.0 g/L was selected as the optimum adsorbent dose for subsequent experiments to ensure maximum dye removal while avoiding unnecessary excess of adsorbent material.

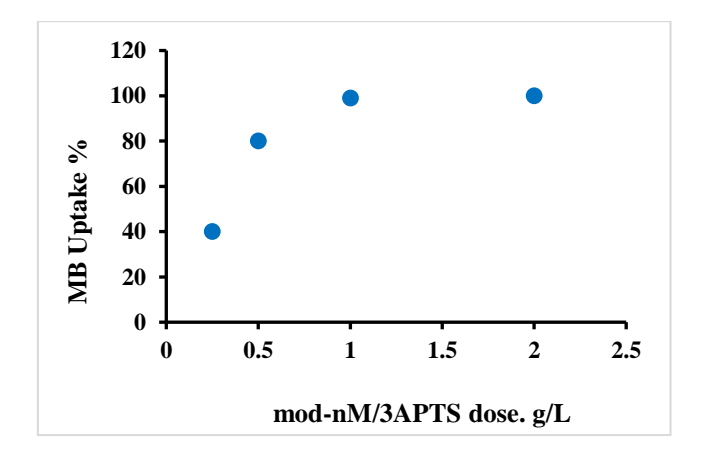


Figure 7. Effect of mod-nM/3APTS dose on MB removal

#### 3.4 Adsorption isotherms

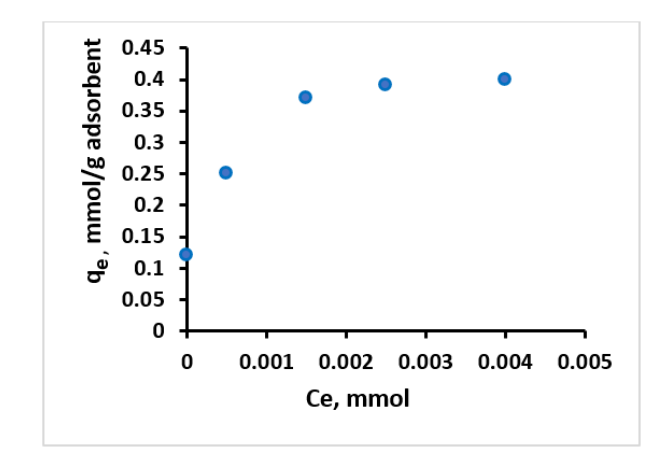
Adsorption isotherm studies are illustrated in Figure 8. The equilibrium adsorption data (qe vs. Ce) showed that the adsorption capacity increased with the equilibrium concentration until reaching a plateau, indicating monolayer adsorption behavior. The linear plot of Ce/qe against Ce (Langmuir plot) confirmed the applicability of the Langmuir isotherm model, as shown in Figure 9. The obtained parameters from the adsorption equations (Eqs. (3) and (4)) are summarized in Table 2. For the Langmuir isotherm, the regression coefficient ( $R^2 = 0.99$ ) was higher compared to the Freundlich isotherm ( $R^2 = 0.95$ ), suggesting that the Langmuir model better describes the adsorption process of MB onto mod-nM/3APTS. The Langmuir adsorption capacity (As) was calculated as 2.50 mmol/g adsorbent, which corresponds to a maximum adsorption capacity of 127.75 mg/g for modnM/3APTS. The K<sub>L</sub> was found to be 8345.6, indicating a strong affinity of the adsorbent towards MB. On the other hand, the Freundlich isotherm yielded values of  $K_F = 0.54$  and n = 14.37, showing favorable adsorption, but with lower correlation compared to the Langmuir model. The modified meerschaum proved to be a highly cost-effective solution for large-scale wastewater treatment, offering several advantages such as the availability and low cost of the raw material, ecofriendliness, ease of modification, high efficiency at low dosage, and convenient handling. These advantages were more pronounced compared with findings reported in the literature, as illustrated in Table 3.

**Table 2.** Sorption capacities and correlation coefficients for MB removal on mod-nM/3APTS

Adsorbent	Freundlich Isotherm			Langmuir Isotherm		
	K <sub>F a</sub>	n	$\mathbb{R}^2$	$K_L$	Asa	$\mathbb{R}^2$
Modification nM/3APTS	0.54	14.37	0.95	8345.6	2.50	0.99

Table 3. Comparative analysis of adsorbents for methylene blue removal

Adsorbent Material	Adsorbent Does (g/L)	Target Adsorbate	Optimal pH	Temperature (°C)	Contact Time (min)	Max. Adsorption Capacity (mg/g)	Authors
Modified Sepiolite	1.03	Acid Green 20 Dye	6.19	25	24.81	58	Malakootian et al. [1]
Cortaderia selloana flower spikes (CSFs)	4	Methylene Blue (MB)	6	25	45	72.99	Parlayıcı et al. [6]
Magnetic C. selloana flower spikes (nM1CSFs)	4	Methylene Blue (MB)	6	25	45	119.0	Parlayıcı et al. [6]
Sycamore (Platanus occidentalis) tree seed pod fibers (STSPF)	2	Methylene Blue (MB)	6	25	125	126.60	Parlayıcı et al. [7]
Zero valent iron immobilized in Sycamore tree seed pod fibers (nZVIOSTSPF)	1	Methylene Blue (MB)	6	25	70	140.80	Parlayıcı et al. [7]
Nodular Sepiolite	12	Ni <sup>2+</sup> Solution	6	25	1440	12.15	Kıpçak et al. [9]
Cellulose Nanowhiskers- based Polyurethane Foam (PUF)	1	Methylene Blue (MB)	7	55	20	110.5	Kumari et al. [12]
Modified Meerschaum	1	Methylene Blue (MB)	8	25	120	127.75	Present study



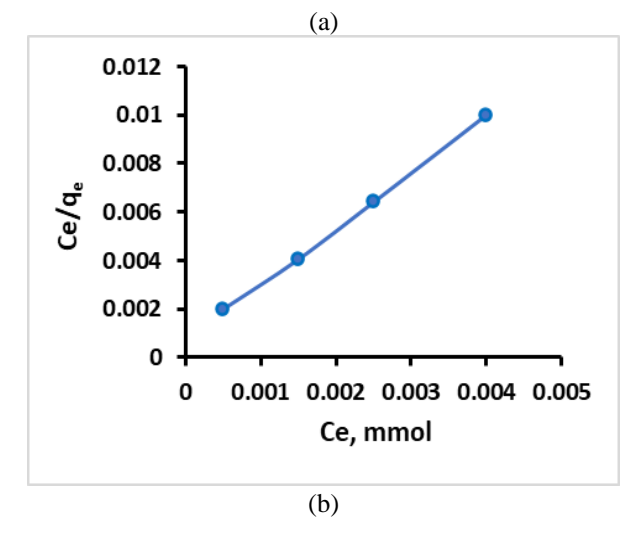


**Figure 8.** Adsorption isotherms of MB on mod-nM/3APTS (a) The relationship between equilibrium concentration (Ce) and adsorption capacity (qe), (b) Langmuir adsorption isotherm plot (Ce/qe vs. Ce) for MB adsorption onto mod-nM/3APTS

#### 3.5 Thermodynamics of adsorption

Considering the thermodynamic implementation of MB on

the surface of mod-nM/3APTS, it is essential to evaluate whether the adsorption phenomenon occurs spontaneously. The effect of temperature on MB adsorption was examined at 25°C, 35°C, 45°C, and 55°C. As shown in Figure 9 and summarized in Table 4, the adsorption capacity of mod-nM/3APTS increased with increasing temperature, suggesting a temperature-dependent behavior.

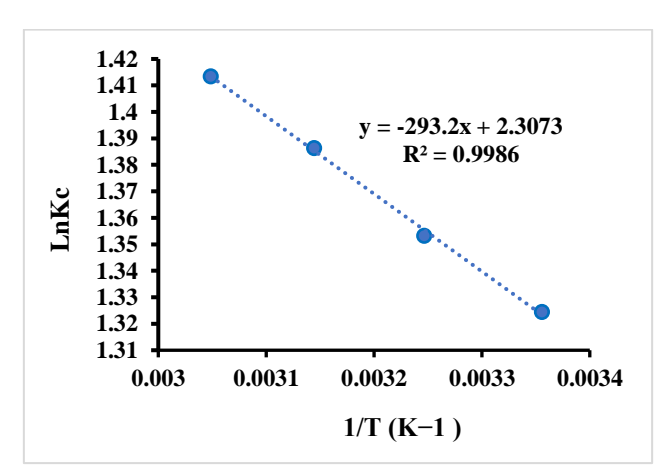


**Figure 9.** The plot of  $K_c$  vs. 1/T for estimation of thermodynamic parameters for MB removal on modnnM/3APTS

To better understand the adsorption mechanism, thermodynamic parameters including Gibbs free energy  $\Delta G^\circ,$   $\Delta H^\circ,$  and  $\Delta S^\circ$  were calculated. The relationship between ln Kc and 1/T (K $^{-1}$ ) is presented in Figure 9, where the linear fit yielded the regression equation:

$$y=-293.2x+2.3073 (R^2=0.9986)$$
 (9)

From the slope  $(-\Delta H^{\circ}/R)$  and intercept  $(\Delta S^{\circ}/R)$ , the enthalpy and entropy values were derived. The negative slope confirms that the adsorption  $\Delta H^{\circ}$  is positive, indicating that the process is endothermic. The positive intercept corresponds to a positive  $\Delta S^{\circ}$ , which implies increased randomness at the

solid–liquid interface and strong affinity between MB molecules and the mod-nM/3APTS surface. The calculated Gibbs free  $\Delta G^{\circ}$  values were negative at all studied temperatures, signifying that the adsorption process is spontaneous. Moreover, the higher negative  $\Delta G^{\circ}$  values at elevated temperatures suggest stronger adsorption at higher thermal energy.

# 3.6 Adsorption kinetics

In order to better understand the adsorption mechanism, kinetic and thermodynamic studies were carried out. The kinetic modeling was performed using pseudo-first-order and pseudo-second-order models (Eqs. (5) and (6)). These models explain the rate-controlling step for dye migration from the aqueous phase to the solid phase and provide insight into the adsorption mechanism. As shown in Table 5, the pseudo-first-order model gave a relatively poor fit with an  $R_2$  value of 0.8808, while the pseudo-second-order model exhibited an excellent correlation with an  $R^2$  of 0.9998. The calculated qe was also much higher for the second-order model (125 mg/g) compared to the first-order model (2.514 mg/g).

Additionally, the rate constant values ( $k_1 = 0.006$ ,  $k_2 = 0.0013$ ) confirm that the pseudo-second-order model provides a better description of the adsorption kinetics. This strongly suggests that the adsorption of MB onto modnM/3APTS is primarily governed by chemisorption, likely involving electron sharing or exchange between the dye

molecules and the aminated silica surface. The presence of amino groups from 3APTS modification enhances these interactions, leading to stronger dye binding. The pseudosecond-order model represents all adsorption steps, including external surface adsorption, film diffusion, intraparticle diffusion, and final attachment to the adsorption sites. Since adsorption occurs rapidly on the outer surface, the slowest stage controlling the overall rate is either film diffusion or pore diffusion within the adsorbent structure.

Thermodynamic parameters derived from adsorption equilibrium data further support these findings (Table 4). The  $\Delta H \circ = +2.44 \text{ kJ mol}^{-1}$  confirms that the adsorption process is endothermic, while the positive  $\Delta S \circ = +19.18 \text{J K}^{-1} \text{ mol}^{-1}$ indicates increased randomness at the solid-liquid interface and strong affinity between MB and mod-nM/3APTS. The Gibbs free  $\Delta G \circ$  was negative at all studied temperatures, ranging from -3.28 to -3.85 kJ mol<sup>-1</sup>, confirming that the adsorption is spontaneous and becomes more favorable with increasing temperature. To evaluate the reusability of modnM/3APTS, desorption experiments were performed using HCl as the regenerating agent. The adsorbent demonstrated excellent stability and reusability, maintaining a high MB removal efficiency. After five regeneration cycles, the adsorption efficiency decreased only slightly, from 93% to 88%, confirming that HCl treatment is effective for regeneration and that mod-nM/3APTS can be applied repeatedly in dye removal processes.

Table 4. Thermodynamic parameters for MB adsorption onto mod-nM/3APTS

Temperature (°C)	*Kabs	R <sup>2</sup> (linear)	$\Delta \mathbf{H}^{\circ}$ (kJ mol $^{-1}$ )	$\Delta S^{\circ}$ (J K <sup>-1</sup> mol <sup>-1</sup> )	$\Delta G^{\circ}$ (kJ mol $^{-1}$ )
25	3.76		2.44	19.18	-3.28
35	3.87	0.000			-3.47
45	4	0.998			-3.67
55	4.11				-3.85

**Table 5.** Kinetic parameters for the adsorption of MB

First-order			Second-order		
k <sub>1</sub>	qe	$\mathbb{R}^2$	$\mathbf{k}_2$	qe	$\mathbb{R}^2$
0.006	2.514	0.8808	0.0013	125	0.9998

# 4. CONCLUSIONS

The study demonstrated that modified nano-meerschaum functionalized with 3-aminopropyl triethoxysilane (mod-nM/3APTS) is a highly effective adsorbent for methylene blue (MB) removal from aqueous solutions. The material achieved a maximum adsorption capacity of 127.75 mg/g at 25°C, with adsorption following the Langmuir isotherm, confirming monolayer coverage. Kinetic analysis revealed that the adsorption process is best described by the pseudo-second-order model, indicating chemisorption as the dominant mechanism. Thermodynamic parameters confirmed the spontaneous and endothermic nature of the adsorption process. Importantly, the adsorbent retained over 88% efficiency after five regeneration cycles, highlighting its durability and reusability.

This research contributes to the development of costeffective and eco-friendly adsorbents by demonstrating the enhanced performance of functionalized meerschaum. The findings establish mod-nM/3APTS as a promising candidate for large-scale wastewater treatment applications, offering high capacity, stability, and reusability for dye removal.

#### **REFERENCES**

- [1] Malakootian, M., Hossaini, H., Asadipour, A., Daneshkhah, M. (2018). Preparation and characterization of modified sepiolite for the removal of Acid green 20 from aqueous solutions: Isotherm, kinetic and process optimization. Applied Water Science, 8(6): 174. https://doi.org/10.1007/s13201-018-0813-8
- [2] Ahmed, Z.M., Radha, M.A., Gubari, M.Q., Mahmoud, M.A., et al. (2025). Recovery of tungsten from catalytic converter scraps using a Schiff-base adsorbent and subsequent preparation of tungsten oxide nanoparticles. Materials Chemistry and Physics, 344: 131146. https://doi.org/10.1016/j.matchemphys.2025.131146
- [3] Tahir, S.S., Rauf, N. (2006). Removal of a cationic dye from aqueous solutions by adsorption onto bentonite clay. Chemosphere, 63(11): 1842-1848. https://doi.org/10.1016/j.chemosphere.2005.10.033
- [4] Zhang, Y.R., Su, P., Huang, J., Wang, Q.R., Zhao, B.X. (2015). A magnetic nanomaterial modified with polylysine for efficient removal of anionic dyes from water. Chemical Engineering Journal, 262: 313-318. https://doi.org/10.1016/j.cej.2014.09.094

- [5] Sharma, P., Borah, D.J., Das, P., Das, M.R. (2016). Cationic and anionic dye removal from aqueous solution using montmorillonite clay: Evaluation of adsorption parameters and mechanism. Desalination and Water Treatment, 57(18): 8372-8388. https://doi.org/10.1080/19443994.2015.1021844
- [6] Parlayıcı, Ş., Pehlivan, E. (2021). Biosorption of methylene blue and malachite green on biodegradable magnetic Cortaderia selloana flower spikes: modeling and equilibrium study. International Journal of Phytoremediation, 23(1): 26-40. https://doi.org/10.1080/15226514.2020.1788502
- [7] Parlayıcı, Ş., Pehlivan, E. (2019). Fast decolorization of cationic dyes by nano-scale zero valent iron immobilized in sycamore tree seed pod fibers: Kinetics and modelling study. International Journal of Phytoremediation, 21(11): 1130-1144.
  - https://doi.org/10.1080/15226514.2019.1606786
- [8] Radha, M.A., Şahin, A., Pehlivan, E., AR, İ. (2019). Inorganic acid doped highly hydroxylated polymer based thin membrane. Materials Today: Proceedings, 18: 1888-1895. https://doi.org/10.1016/j.matpr.2019.06.678
- [9] Kıpçak, İ., Ersal, E.K., Özdemir, M. (2020). Adsorptive removal of Ni2+ ions from aqueous solutions by nodular sepiolite (meerschaum) and industrial sepiolite samples from Eskişehir, Turkey. Clays and Clay Minerals, 68(3): 220-236. https://doi.org/10.1007/s42860-020-00077-7
- [10] Rosales, E., Pazos, M., Sanromán, M.A., Tavares, T. (2012). Application of zeolite-Arthrobacter viscosus system for the removal of heavy metal and dye: chromium and Azure B. Desalination, 284: 150-156. https://doi.org/10.1016/j.desal.2011.08.049
- [11] Wang, Q., Wang, Y., Chen, L. (2019). A green composite hydrogel based on cellulose and clay as efficient absorbent of colored organic effluent. Carbohydrate Polymers, 210: 314-321. https://doi.org/10.1016/j.carbpol.2019.01.080
- [12] Kumari, S., Chauhan, G.S., Ahn, J.H. (2016). Novel cellulose nanowhiskers-based polyurethane foam for rapid and persistent removal of methylene blue from its aqueous solutions. Chemical Engineering Journal, 304: 728-736. https://doi.org/10.1016/j.cej.2016.07.008
- [13] Yu, H., Zhu, Y., Xu, J., Wang, A. (2020). Fabrication porous adsorbents templated from modified sepiolitestabilized aqueous foams for high-efficient removal of cationic dyes. Chemosphere, 259: 126949. https://doi.org/10.1016/j.chemosphere.2020.126949
- [14] Gong, X., Huang, D., Liu, Y., Zeng, G., Wang, R., Wei, J., Zhang, C. (2018). Pyrolysis and reutilization of plant residues after phytoremediation of heavy metals contaminated sediments: For heavy metals stabilization and dye adsorption. Bioresource Technology, 253: 64-71. https://doi.org/10.1016/j.biortech.2018.01.018
- [15] He, D., Huang, H., Xu, W., Qin, F., Liu, S. (2018). Adsorption properties and mechanism of purified palygorskite on methylene blue. Arabian Journal of Geosciences, 11(21): 658. https://doi.org/10.1007/s12517-018-4015-3
- [16] Çoruh, S., Elevli, S., Doğan, G. (2017). Optimization study of adsorption of crystal violet and Congo red onto sepiolite and clinoptilolite. Global Nest Journal, 19(2): 336-343. https://doi.org/10.30955/gnj.002128
- [17] Zhuang, G.Z., Zhang, Z.P., Chen, H.W. (2018). Influence of the interaction between surfactants and

- sepiolite on the rheological properties and thermal stability of organo-sepiolite in oil-based drilling fluids. Microporous and Mesoporous Materials, 272: 143-154. https://doi.org/10.1016/j.micromeso.2018.06.017
- [18] Raya, J., Hirschinger, J., Ovarlez, S., Giulieri, F., Chaze, A.M., Delamare, F. (2010). Insertion of indigo molecules in the sepiolite structure as evidenced by 1h–29si heteronuclear correlation spectroscopy. Physical Chemistry Chemical Physics, 12(43): 14508-14514. https://doi.org/10.1039/C0CP00834F
- [19] Alkan, M., Demirbaş, Ö., Doğan, M. (2007). Adsorption kinetics and thermodynamics of an anionic dye onto sepiolite. Microporous and Mesoporous Materials, 101(3): 388-396. https://doi.org/10.1016/j.micromeso.2006.12.007
- [20] Pardo, L., Cecilia, J.A., López-Moreno, C., Hernández, V., Pozo, M., Bentabol, M.J., Franco, F. (2018). Influence of the structure and experimental surfaces modifications of 2:1 clay minerals on the adsorption properties of methylene blue. Minerals, 8(8): 359. https://doi.org/10.3390/min8080359
- [21] Sarossy, Z., Blomfeldt, T.O., Hedenqvist, M.S., Koch, C.B., Ray, S.S., Plackett, D. (2012). Composite films of arabinoxylan and fibrous sepiolite: Morphological, mechanical, and barrier properties. ACS Applied Materials & Interfaces, 4(7): 3378-3386. https://doi.org/10.1021/am3002956
- [22] Al-Abboodi, H., Fan, H., Al-Bahrani, M., Abdelhussien, A., Mohamad, B. (2024). Mechanical characteristics of nano-crystalline material in metallic glass formers. Facta Universitatis-Series Mechanical Engineering, 22(2): 315-328. https://doi.org/10.22190/FUME230128016A
- [23] Mahdavinia, G.R., Hosseini, R., Darvishi, F., Sabzi, M. (2016). The release of cefazolin from chitosan/polyvinyl alcohol/sepiolite nanocomposite hydrogel films. Iranian Polymer Journal, 25(11): 933-943. https://doi.org/10.1007/s13726-016-0480-2
- [24] Ma, Y., Wu, X., Zhang, G. (2017). Core–shell Ag@Pt nanoparticles supported on sepiolite nanofibers for the catalytic reduction of nitrophenols in water: Enhanced catalytic performance and DFT study. Applied Catalysis B: Environmental, 205: 262-270. https://doi.org/10.1016/j.apcatb.2016.12.025
- [25] Na, C. (2020). Size-controlled capacity and isocapacity concentration in Freundlich adsorption. ACS Omega, 5(22): 13130-13135. https://doi.org/10.1021/acsomega.0c01144
- [26] Mutavdžin, I., Seidel-Morgenstern, A. (2024). Estimating the parameters of competitive Langmuir adsorption isotherms from measured responses to rectangular pulse injections exploiting equilibrium theory. Adsorption, 30(3): 337-349. https://doi.org/10.1007/s10450-024-00436-z
- [27] Tran, H.N., Lima, E.C., Juang, R.S., Bollinger, J.C., Chao, H.P. (2021). Thermodynamic parameters of liquid–phase adsorption process calculated from different equilibrium constants related to adsorption isotherms: A comparison study. Journal of Environmental Chemical Engineering, 9(6): 106674. https://doi.org/10.1016/j.jece.2021.106674
- [28] Sultan, S., Abed, F.N.M., Irzoqy, M.E. (2022). Mr Removal some types of heavy metals using kind biofungi. NTU Journal of Renewable Energy, 2(1): 34-38. https://doi.org/10.56286/ntujre.v2i1.211

- [29] Yagub, M.T., Sen, T.K., Afroze, S., Ang, H.M. (2014). Dye and its removal from aqueous solution by adsorption: A review. Advances in Colloid and Interface Science, 209: 172-184. https://doi.org/10.1016/j.cis.2014.04.002
- [30] Zhang, J., Yan, Z., Ouyang, J., Yang, H., Chen, D. (2018). Highly dispersed sepiolite-based organic modified nanofibers for enhanced adsorption of Congo
- red. Applied Clay Science, 157: 76-85. https://doi.org/10.1016/j.clay.2018.02.031
- [31] Al-abady, F., Tapabashi, N., Bahjat, A. (2019). Study of thermodynamic and kinetic adsorption of azo dyes on different adsorbent surfaces. Kirkuk Journal of Science, 14(2): 273-296.

https://doi.org/10.32894/kujss.2019.14.2.16